Article

Discovery Medicine 2023; 35(175): 131–143
https://doi.org/10.24976/Discov.Med.202335175.14

The Unique Genetic Mutation Characteristics Based on Large Panel Next-Generation Sequencing (NGS) Detection in Multiple Primary Lung Cancers (MPLC) Patients

Zhu Liang[1,2], Guoxiong Zeng[3], Wang Wan[3], Biao Deng[3], Chunyuan Chen[2], Fasheng Li[2], Guanzhou Lin[3], Yuying Lin[3], Haitao Lin[4], Guixi Mo[5,*], Huilai Miao[1,6,*]

[1]The First Affiliated Hospital, Jinan University, 510630 Guangzhou, Guangdong, China
[2]Department of Thoracic Surgery, Affiliated Hospital of Guangdong Medical University, 524000 Zhanjiang, Guangdong, China
[3]Guangdong Medical University, 524000 Zhanjiang, Guangdong, China
[4]Health Management Center, Affiliated Hospital of Guangdong Medical University, 524000 Zhanjiang, Guangdong, China
[5]Department of Anesthesiology, Affiliated Hospital of Guangdong Medical University, 524000 Zhanjiang, Guangdong, China
[6]Department of Hepatobiliary Surgery, The Second Affiliated Hospital of Guangdong Medical University, 524000 Zhanjiang, Guangdong, China
*Correspondence: miaohuilai@outlook.com (Huilai Miao); moguixi904015600@hotmail.com (Guixi Mo)
Published: 1 April 2023

Background: With the wide application of multislice spiral computed tomography (CT), the frequency of detection of multiple lung cancer is increasing. This study aimed to analyze gene mutations characteristics in multiple primary lung cancers (MPLC) using large panel next-generation sequencing (NGS) assays.

Methods: Patients with MPLC surgically removed from the Affiliated Hospital of Guangdong Medical University from Jan 2020 to Dec 2021 enrolled the study. NGS sequencing of large panels of 425 tumor-associated genes was performed.

Results: The 425 panel sequencing of 114 nodules in 36 patients showed that epidermal growth factor receptor (*EGFR*) accounted for the largest proportion (55.3%), followed by Erb-B2 Receptor Tyrosine Kinase 2 (*ERBB2*) (9.6%), v-Raf murine sarcoma viral oncogene homolog B1 (*BRAF*), and Kirsten rat sarcoma viral oncogene (*KRAS*) (8.8%). Fusion target variation was rare (only 2, 1.8%). *ERBB2* Y772_A775dup accounted for 73%, *KRAS* G12C for about 18%, and *BRAF* V600E for only 10%. AT-rich interaction domain 1A (*ARID1A*) mutations were significantly higher in invasive adenocarcinoma (IA) which contained solid/micro-papillary malignant components ($p = 0.008$). The tumor mutation burden (TMB) distribution was low, with a median TMB of 1.1 MUTS/Mb. There were no differences in the TMB distribution of different driver genes. In addition, 97.2% of MPLC patients (35/36) had driver gene mutations, and 47% had co-mutations, mainly in IA (45%) and invasive adenocarcinoma (MIA) (37%) nodule, with *EGFR* (39.4%), *KRAS* (9.1%), *ERBB2* (6.1%), tumor protein 53 (*TP53*) (6.1%) predominately.

Conclusions: MPLC has a unique genetic mutation characteristic that differs from advanced patients and usually presents with low TMB. Comprehensive NGS helps to diagnose MPLC and guides the MPLC clinical treatment. *ARID1A* is significantly enriched in IA nodules containing micro-papillary/solid components, suggesting that these MPLC patients may have a poor prognosis.

Keywords: multiple primary lung cancer (MPLC); next-generation sequencing (NGS); mutational signature; genomic diagnosis; adenosquamous carcinoma of the lung

Introduction

Currently, lung cancer is the second most common malignancy in new diagnosed cancer cases worldwide (11.4% of all new cases) and remains the leading cause of cancer deaths (18.0% of all cancer deaths) [1]. In China, it still ranks first in the list of cancer incidence and mortality [2,3]. Multiple primary lung cancers (MPLC) account for 5 to 20% of lung cancers [4,5]. MPLC is detected more frequently due to the widespread use of computed tomography (CT), fluorescent endoscopy, and positron emission tomography [6,7]. The diagnosis and treatment of isolated primary lung adenocarcinoma are well established. However, from a clinical pathological point of view, identifying malignancies at the onset of the disease is a challenge and needed. The prognosis is expected to be better in patients with independent primary tumors than in patients with intrapulmonary metastases (IM) [8,9].

With the development of high-throughput sequencing techniques, mutation analysis of specific driver and inhibitory genes helps distinguishing between multiple primary tumors and lung metastases [10]. Many reports

have shown inconsistencies between paired primary and metastatic lung cancer specimens with epidermal growth factor receptor (*EGFR*) and Kirsten rat sarcoma viral oncogene (*KRAS*) mutations, suggesting tumor heterogeneity. This was shown by one metaanalysis which found a high rate of inconsistencies between *EGFR* and *KRAS* mutations (about 15%) [11].

Next-generation sequencing (NGS) platforms have been widely implemented in clinical diagnostic laboratories. NGS provides mutation analysis with higher analytical sensitivity to detect mutations, lower allele frequencies and a more comprehensive range of reportable mutations [12]. Distinguishing between MPLC and IM is crucial for clinicians treating patients MPLC to select the appropriate treatment strategy and accurately predict patients' prognosis. In this study, the characteristics of gene mutations in MPLC were analyzed by NGS large panel detection, which provides clinical guidance for diagnosing and treating MPLC.

Materials and Methods

Patient Selection and Data Collection

Patients with surgically removed multiple non-small cell lung cancer (NSCLC) that were in the Affiliated Hospital of Guangdong Medical University from Jan 2020 to Dec 2021 enrolled the study. Inclusion criteria was as follows: (a) Clinical diagnosis of primary lung cancer and adenocarcinoma in situ (AIS) was established; (b) Surgery to remove more than 2 malignant lesions; (c) Age $\geq$18 years; (d) All patients are newly treated. Exclusion criteria was: (a) Patients with other primary malignant tumors; (b) Patients with apparent liver and kidney dysfunction, immune system, and hematologic system diseases.

The patients' clinical features were collected, including sex, age, smoking history, surgical modality, tumor location, postoperative pathological outcomes, International Association for the Study of Lung Cancer (IASLC) grading, tumor stage, CT components, consolidation tumor ratio (CTR) and special CT image (lobes, burrs, cavities, pleural traction, vessel penetration, etc.). Pathological staging of individual lesions of MPLC was performed by IASLC guidelines 2016. Lung cancer staging was based on International Union Against Cancer (UICC) 8th Edition Tumor Node Metastasis (TNM) staging.

DNA Extraction and Sequencing Library Preparation

For each patient, a sample of formaldehyde-fixed paraffin-embedded (FFPE) tumor tissue obtained by endoscopic biopsy before treatment was taken for DNA extraction. Pathologists confirmed that all samples had a tumor content was at least 10%. Eight 10 μm FFPE slices were dewaxed with xylene, and then the genomic DNA was extracted using the QIAamp DNA FFPE Tissue Kit (166046348, Qiagen, Hilden, Germany). The amount and quality of DNA were assessed using a Qubit 3.0 fluorometer and a Nanodrop 2000 (AZY1601637, Thermo Fisher Scientific, Waltham, MA, USA). Genomic DNA sonication was then broken into 350 bp fragments using the Covaris M220 ultrasound system and purified with Agencourt AMPure XPbeads (26220001, Beckman Coulter, Mississauga, Canada).

DNA fragments library preparation after ultrasound fragmentation was made using the KAPA hyper library preparation kit (0000109693, KAPA Biosystems, Wilmington, MA, USA). Libraries with different molecular tags were mixed. The hybrid libraries were targeted and enriched with Integrated DNA Technologies (IDT) xGen Lockdown Reagents and custom probes (0000593655, IDT, Coralville, IA, USA), which covered exon regions of 425 genes and introns of 57 fusion genes. The enriched library was amplified using Illumina p5 (5′-AATGATACGACCACCGA-3′), and p7 (5′-CAAGCAGAAGACGGCATACGAGAT-3′) primers and KAPA Hifi Hot-Start ReadyMix (0000121538, KAPA Biosystems, Wilmington, MA, USA), then, AgencourtAMPure XPbeads Purification were performed. The sequencer library was then quantitatively sequenced using the KAPALibrary Quantification kit (0000103958, KAPA Biosystems, Wilmington, MA, USA) by the qPCR (quantitative polymerase chain reaction) method, and the fragment size distribution was examined using Bioanalyzer2100 (DE54108086, Agilent Technologies, Stanta Clara, CA, USA). The final library was sequenced using the Illumina Hiseq 4000 platform, with an average sequencing depth of at least 250×.

Sequencing Data Analysis

Sequencing Data was analyzed by a validated automated process of Gene Biogene, main steps are described below. BCK2fastq (92122, San Diego, CA, USA) was used for data splitting, and then FASTQ file quality filtering (QC) was performed with Trimmomatic. Low-mass based (based on Phred score below 20) or N bases were removed. Burrows-Wheller Aligner (BWA-mem, version0.7.12, Palo Alto, CA USA) was used to compare the measured sequences with the human reference genome *HG19*. Picard was used to remove the repetitive sequences caused by PCR. Genome Analysis Toolkit (GATK version3.4.0, Broad Institute, Cambridge, MA, USA) was used to perform local assembly correction comparisons around the insertion-deletion and the base mass fraction was recalibrated. Single nucleotide variant (SNV) and insertion/deletion mutations were determined using VarScan2 software (version2.4.4, MD Anderson Cancer Center, Oxford, UK), with the parameters as follows: Minimum sequencing depth = 20, minimum base mass = 25, minimum variant allele frequency (VAF) = 0.03, minimum variation support reading = 3, both positive and negative chains measured variation, and chain bias of no more than 10%.

Table 1. Patient characteristics.

Characteristics	N	(%)
Median age, years [range]	57 (33–82)	
Gender		
Female	25	69.4
Male	11	30.6
History of smoking		
Yes	3	8.3
No	33	91.7
Number of nodules		
2	20	55.6
≥3	16	44.4
Spatial distribution of nodules		
Ipsilateral lung with lung segment	11	30.6
Ipsilateral lung segments are different	18	50.0
Different lateral lungs	7	19.4
Stages		
0	1	2.8
Ia	29	80.6
Ib	3	8.3
≥II	3	8.3

Table 2. Tissue characteristics.

Characteristics	N	(%)
Size (mm)		
<5	25	21.9
5–15	70	61.4
>15	19	16.7
Histology		
AIS	32	28.1
MIA	48	42.1
IA	32	28.1
Other	2	1.8
Stage		
0	32	28.1
Ia1	55	48.2
Ia2	12	10.5
Ia3	5	4.4
Ib	3	2.6
≥II	5	4.4
None	2	1.8
CTR		
Pure GGN (CTR = 0)	61	53.5
0 < CTR < 0.5	28	24.6
0.5 < CTR < 1	10	8.8
Solid (CTR = 1)	14	12.3
Unknow	1	0.9

AIS, adenocarcinoma in situ; MIA, minimally invasive adenocarcinoma; IA, invasive adenocarcinoma; GGN, ground glass nodule.

Droplet digital polymerase chain reaction (ddPCR) was used to validate the copy number variation (CNV) program using 38 samples. System noise in copy number data was reduced by principal component analysis of 100 standard samples in the same batch. The assay program could detect 0.4× copy loss at ≥50% tumor cell content and 4× copy number increase at ≥10%. Log_2 multiples change rate ≥0.67 was used to detect CNV repetitions, while log_2 multiples change rates ≤–0.74 were used to detect CNV deletions.

In the next filtering step, only Catalogue of Somatic Mutations in Cancer (COSMIC) hotspots with a VAF above 1% and at least 3 mutation readings (recurrence ≥20) mutations, or other mutations with at least 5 supporting readings, were read out.

Statistical Methods

The bioinformatics analysis platform of Nanjing Shihe Gene Biotechnology Co., Ltd. was used to identify gene variations, comment on mutations, filter variations, and comprehensive mutation information, such as mutations, fusions, and amplification deletions at 425 gene points. Mutation mapping was performed using the R statistical analysis package (R version3.5.3) and mutation distribution was done using cBioPortal online (http://www.cbioportal.org). The statistical difference of two groups and three groups were tested with Fisher's exact test. $p < 0.05$ was considered statistically significant.

Results

Patient and Tissures Characteristics

Patient characteristics are presented in Table 1. Our study included 36 patients with multiple pulmonary nodules, including 11 men (30.6%) and 25 women (69.4%), with a median age of 57 years (range: 33 to 82 years). Of those, 3 (8.3%) patients were smoker and 33 (91.7%) non-smokers. Among them, 20 had 2 lung lesions removed, and 16 had more than 3 lung lesions removed. 11 cases (30.6%) occurred in the same lung segment of the ipsilateral lung, 18 cases (50.0%) occurred in different lung segments of the ipsilateral lung, and 7 cases (19.4%) occurred in different lateral lungs. A total of 114 lesions were available for this study, including 112 lung adenocarcinomas. There was 1 patient (2.8%) in stage 0, 29 patients in stage Ia (80.6%), 3 patients in stage Ib (8.3%), and 3 patients above stage II (8.3%).

Among the 114 tissues, we found 95 (83.3%) tissues ≤15 mm and 104 (91.2%) ≤ stage Ia. In addition, non-invasive nodules (AIS + MIA) accounted for 70.2% (80/114), and pure ground glass nodule (GGN) accounted for 53.5% (61/114). More characteristics details are listed in Fig. 1A and Table 2.

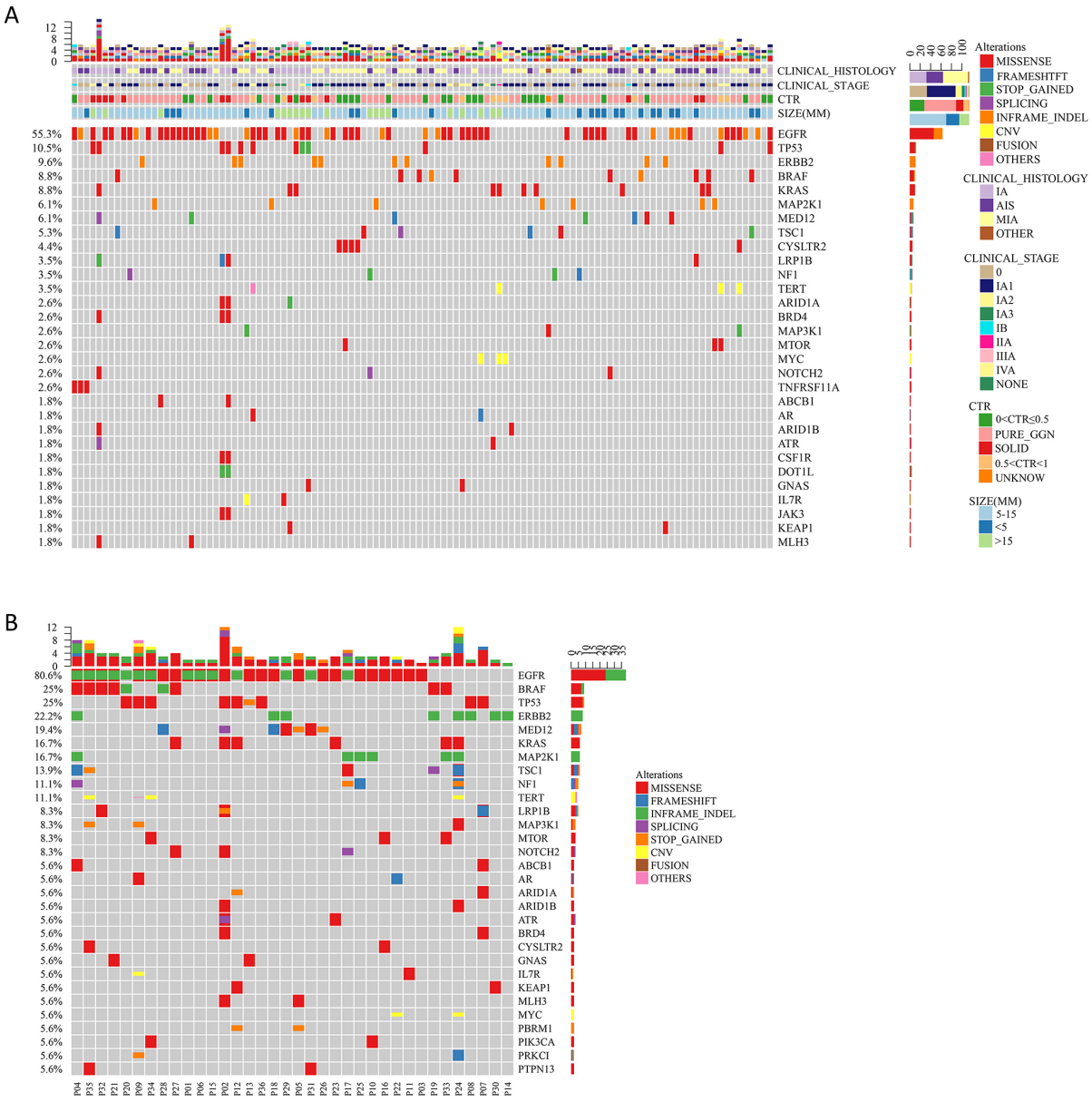

Fig. 1. Genetic profiles in sample tissues and patients. (A) Genetic profiles in 114 sample tissues. Oncoprint depicts stage, histology, size, CT ingredients and genetic panel. Each column represents one tissue. Total number of mutations detected in each tissue was graphed on top of the Oncoprint. The right-side bar shows the number of tissues. Mutation detection rate of each gene is on the left. CTR, consolidation tumor ratio. (B) Genomic profile in 36 patients. Total number of mutations detected in each patient were graphed on top of the Oncoprint. The right-side bar shows the number of patients. The mutation detection rate of each gene is on the left.

Mutation Spectrum and Mutation Signal

Analysis of multiple nodular mutation types showed that the types of missense mutations and deletion/insertion mutations were dominant. Overall, 68% of missense mutations and 12% of deletion/insertion mutations. The forms of base mutations were C > T, C > A, and T > G, accounting for 28%, 25%, and 24%, respectively.

114 Sample Tissues Genetic Mutation Analysis

Among the 36 patients, there were 114 sample tissues, with the highest rate of *EGFR* gene mutation among all samples (55.3%), followed by tumor protein 53 (*TP53*) (10.5%) and Erb-B2 Receptor Tyrosine Kinase 2 (*ERBB2*) (9.6%) (Fig. 1A). It was found that Bromodomain-Containing Protein 4 (*BRD4*) co-occurred significantly with low density lipoprotein-related protein 1B (*LRP1B*)/*DOT1L* (*DOT1L* was the same patient with

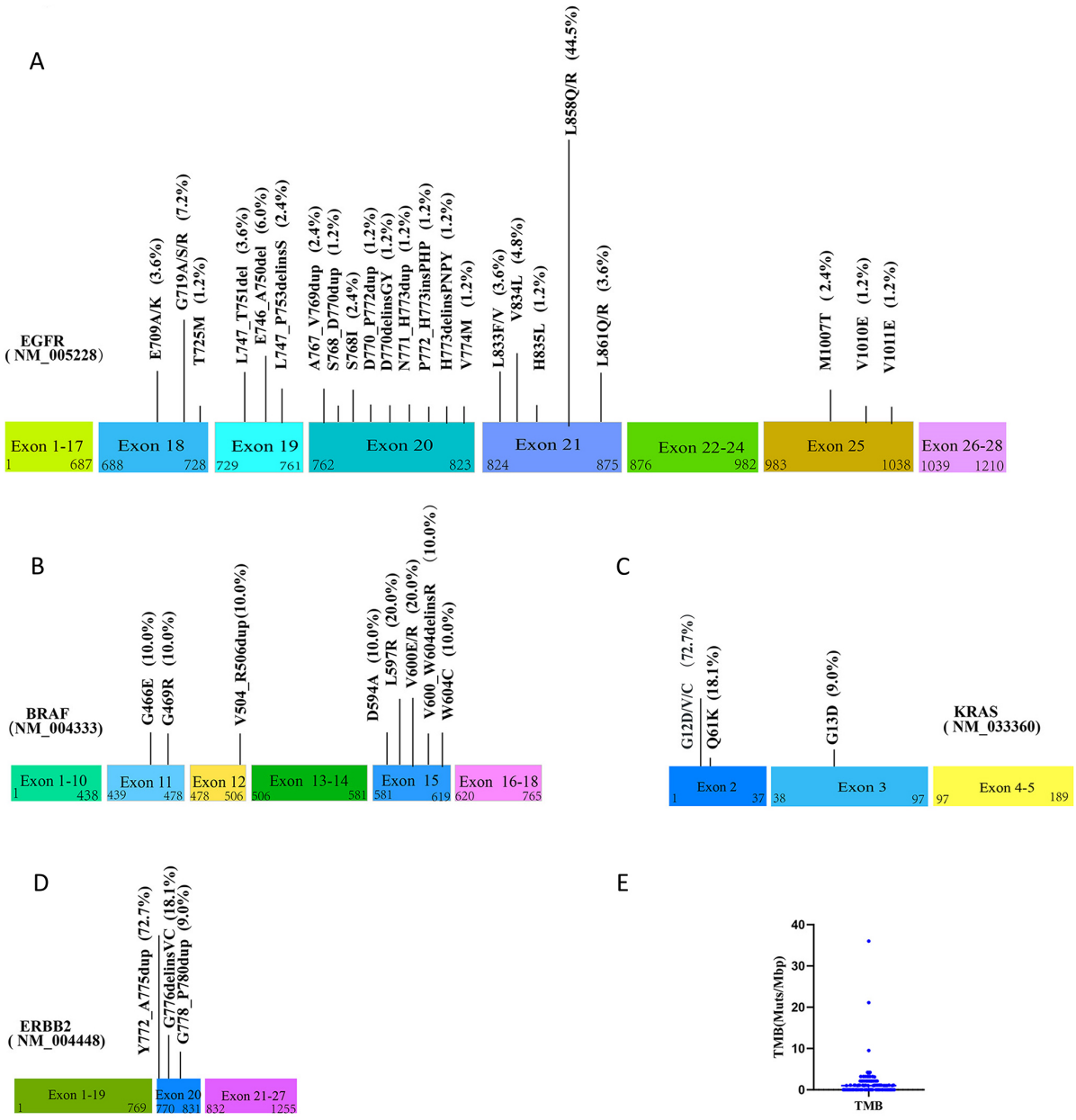

Fig. 2. Genetic mutations in 114 sample tissues. (A) *EGFR* gene mutation distribution characteristics analysis. (B) *BRAF* gene mutation distribution characteristics. (C) *KRAS* gene mutation distribution characteristics. (D) *ERBB2* gene mutation distribution characteristics. (E) TMB distribution in 114 tissues.

two different mutation forms repeated) ($p < 0.01$) and AT-rich interaction domain 1A (*ARID1A*) with *DOT1L* ($p < 0.01$). There was no significant mutually exclusive genetic variation.

Among the 11 drug target genes concerned in NSCLC, *EGFR* mutations incidence accounted for 55.3% of the 114 multiple nodules, followed by *ERBB2* (9.6%), v-Raf murine sarcoma viral oncogene homolog B1 (*BRAF*) (8.8%), *KRAS* (8.8%), c-ros oncogene 1(*ROS1*) (1.8%), anaplastic lymphoma kinase (*ALK*) (0.9%). There was no mesenchymal-epithelial transition factor (*MET*) amplification. *ALK* fusion and *ROS1* fusion were in 1 case each, and no rearranged during transfection (*RET*) fusion and neurotrophic tyrosine receptor kinase (*NTRK*) 1/2/3 fusion was found (**Supplementary Fig. 1**). There were 83 *EGFR* mutations detected in 63 nodule samples. Among them, 48 were exon 21 mutations, accounting for 58% of all *EGFR* mutations. Exon 19, 20, 18, and 25 mutations accounted for 12%, 13%, 12%, and 5% of all *EGFR* mutations, respectively.

Further analyzing the most common MPLC gene mutation subtypes, we found that the *EGFR* exon 20 and 21 mutations were the most abundant, with 9 and 8 mutations,

Table 3. Major types of mutations in different pathological subtypes.

AIS		MIA		IA	
Gene Name	Frequency (%)	Gene Name	Frequency (%)	Gene Name	Frequency (%)
EGFR	34.4	*EGFR*	56.3	*EGFR*	78.1
BRAF	28.1	*ERBB2*	14.6	*TP53*	34.4
MAP2K1	12.5	*CYSLTR2*	10.4	*KRAS*	18.8
TSC1	9.4	*MED12*	8.3	*ARID1A*	9.4
KRAS	9.4	*MAP2K1*	6.2	*BRD4*	9.4
MED12	6.2	*TSC1*	6.2	*LRP1B*	9.4

respectively. Among them, exon 21 mutation was mainly concentrated in the L858 locus with a mutation ratio of 77%. Exon 19 mutations were all insertion/deletion mutations. The leading mutation site was E746_750del, accounting for 50%. Exon 18 mutation site was G719, accounting for 60% (Fig. 2A). *BRAF* main mutation site was L597R, accounting for 20%, while V600E accounts for only 10% (Fig. 2B). Furthermore, *KRAS* leading mutation site was G12, accounting for about 18% (Fig. 2C). *ERBB2* mutations were all exon 20 insertion/deletion mutations, of which the main mutation site was Y772_A775dup, accounting for 73% (Fig. 2D).

Mutations in Nodules with Different Clinical Pathological Features

The primary mutation types of nodules in different pathological subtypes are shown in Table 3. We found that the highest frequency of gene mutations in the three different pathological subtypes (AIS, MIA, IA) was the *EGFR* gene. The highest mutation frequency in the IA group accounted for 78.1%. In addition, we found that *EGFR*/*TP53*/*KRAS* was more abundant in sample tissues in the IA group, *BRAF* was enriched in AIS, and the frequency of *EGFR* and *TP53* mutations increased significantly following the degree of malignancy of pathological subtypes (Fig. 3A). Among the 32 IA sample tissues, 7 had solid/micro-papillary components. *ARID1A* mutations were significantly higher in IA containing solid/micro-papillary malignant components ($p = 0.008$) (Fig. 3B). In addition, *ARID1A* gene mutations incidence in the IASLC 3 group was 75% ($p = 0.02$) (Fig. 3C).

According to the top6 gene in the nodule size (<5 mm, 5–15 mm, >15 mm) analysis and pathological stage (0, Ia1, Ia2, Ia3), it was found that the larger the nodule, the more frequent the *TP53* occurrence and *KRAS* frequency occurrence increased significantly (Fig. 4A). With the increase of nodular staging, *EGFR* and *TP53* incidence increased significantly, *BRAF* decreased significantly (Fig. 4B). Our results showed that *BRAF* mutations were significantly higher in pure ground glass, and *KRAS*, *TP53*, and *ARID1A* were significantly higher in solid, CTR >0.5, or nodules with specific imaging features (Fig. 4C–E).

TMB Analysis of 114 Sample Tissues

TMB (tumor mutation burden) was analyzed in 114 tissues. A TMB low distribution, with a median TMB of 1.1 Mutations per Megabase (MUTS/Mb) was found (Fig. 2E). There were no differences in the TMB distribution between different driver genes, but *ERBB2* 20ins had a downward trend. In different *EGFR* subtypes (L858R, 19DEL, 20ins, 18 mutation), *EGFR* 18exon TMB was significantly higher than that of the 20ins mutation ($p = 0.02$). It was found that the TMB of IA was significantly higher than that of AIS ($p = 0.046$) and MIA ($p = 0.02$). In addition, the IASLC 3 group TMB was also higher than that of IASLC 1 and 2.

With the increase in nodules diameter, TMB distribution tended to increase. TMB of >15 mm nodules was significantly higher than that of the <5 mm nodules ($p = 0.001$). Moreover, TMB distribution of nodules with CTR >0.5 was significantly higher ($p = 0.0002$), especially in solid nodules. However, no correlation between TMB and nodular staging was observed.

Genetic Mutations in 36 Patients Analysis

Gene mutation profiles of all nodule samples from 36 patients was analyzed with a high proportion of *EGFR* mutations (80.6%), followed by *BRAF* (25%), *TP53* (25%), and *ERBB2* (22.2%) (Fig. 1B). Among them, Neurofibromin 1(*NF1*) and mitogen-activated protein kinase kinase 1(*MAP2K1*), and *MAP3K1* and telomerase reverse transcriptase (*TERT*) coexist significantly ($p < 0.05$). The top6 gene was analyzed in groups according to the number of patients with 2 and ≥3 nodules. *TP53* was significantly enriched in patients with 2 nodules, and *BRAF*/*MAPK1*/Tuberous Sclerosis Complex 1 (*TSC1*) was significantly enriched in patients with more than 3 nodules (Fig. 5A). According to the proportion of IA nodules in the total number of resected nodules, each patient was divided into two groups, <50% IA and ≥50% IA, and the top6 genes were analyzed. *TP53* was significantly enriched in patients with IA accounting for more than 50% ($p < 0.01$). *MAP2K1* was significantly enriched in less than 50% of patients with IA ($p < 0.01$) (Fig. 5B).

Among the 36 patients, 35patients (97.2%) had driver gene mutations. The number of drive gene mutations involved in each patient ranged from 1 to 4, with a median

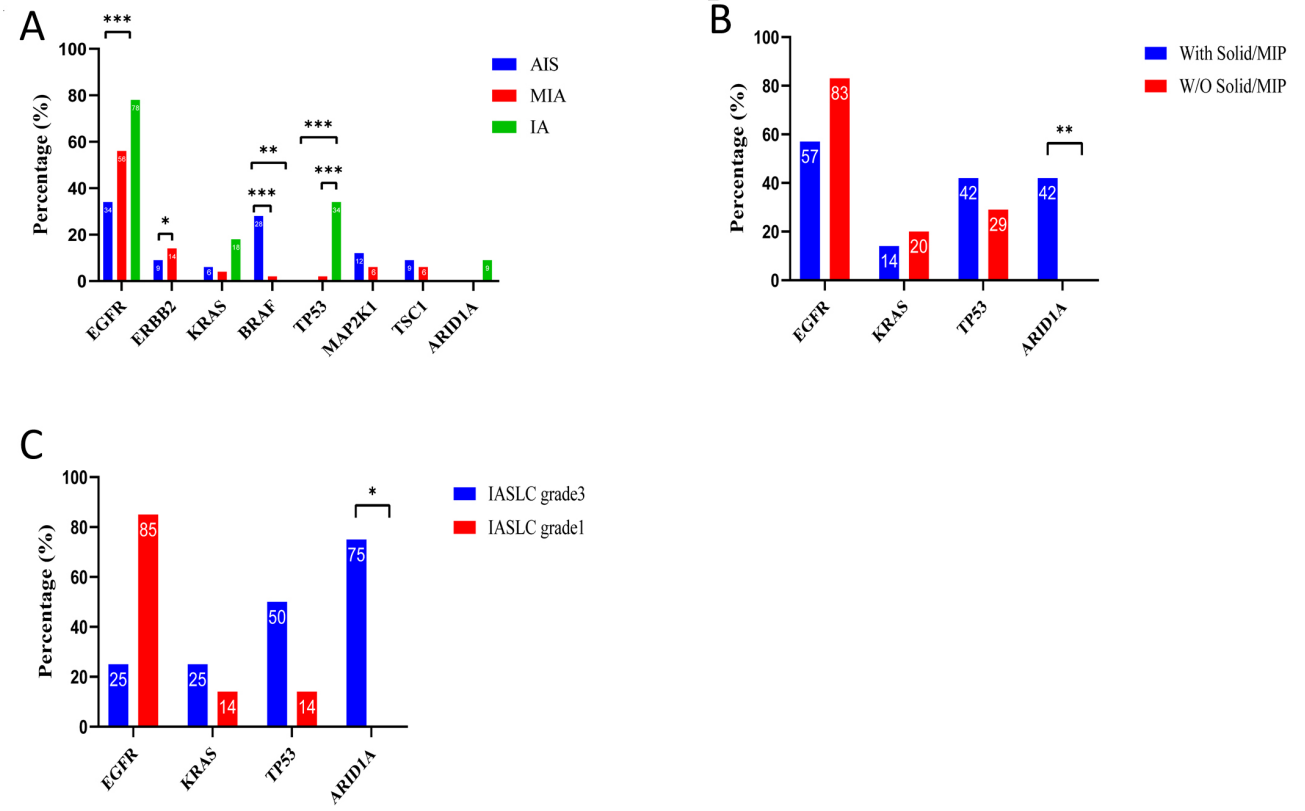

Fig. 3. Analysis of pathology and genetic mutations in 114 sample tissues. (A) Major mutant genes in nodule samples of different pathological subtypes analysis. (B) Major mutant genes in nodule samples with and without micropapillary component in group IA analysis. W/O Solid/MIP, without solid/micro-papillary. (C) Major mutations in different IASLC grades. $^{*}p < 0.05$; $^{**}p < 0.01$; $^{***}p < 0.001$.

of 1. *EGFR* single gene accounted for the most significant proportion of diver genes (46%), followed by *EGFR* + *BRAF* (14%), *EGFR* + *ERBB2* (9%), *EGFR* + *KRAS* (8%), and *ERBB2* (8%) (Fig. 6A). It was observed that patients with the highest pathological subtype of IA might have had more driver gene mutations. The highest number of driver gene mutations ($p = 0.007$) was observed in IASLC level 3 patients (Fig. 6B). The number of patient-driven gene mutations distribution may not be related to the diameter, location, and stage ($p > 0.05$). Moreover, TMB in patients tended to increase with in IASLC grading and staging (Fig. 6C,D).

Although the median number of co-mutant genes was 0 in 36 patients with multiple nodules, 47% of patients still had co-mutations, and 21% had more than two co-mutations. Seventeen co-mutant patients had 73 co-mutant gene nodules, and co-mutant nodules mainly occurred in IA (33, 45%) and MIA (37%) nodule types. A total of 85% of patients were single-base variants, including T > G (35.7%), C > A (28.6%), and C > T (25%). These results show that co-mutant genes may be more likely to occur in patients with air cavity dissemination and pleural invasion, especially air cavity dissemination. More than 2 co-mutant genes were significantly enriched in patients with air cavity dissemination ($p < 0.05$) (Fig. 5C). Patients with IASLC 3 had a higher probability of more than 2 co-mutations (Fig. 5D). 47.2% patients (17/36) had co-mutations, of which the top 5 genes accounted for *EGFR* (39.4%), *KRAS* (9.1%), *ERBB2* (6.1%), *TP53* (6.1%), *DOT1L* (6.1%) (**Supplementary Fig. 2A**). The first 4 mutation sites of co-mutant genes were functional mutations, except for *EGFR* M1007T. There were 9 patients with *EGFR* co-mutation with 11 co-mutation sites, of which L858R accounted for the largest proportion (82%) (**Supplementary Fig. 2B)**.

Discussion

Evaluation of the genomic profile of multiple lung adenocarcinomas complements histological findings by enabling a more comprehensive assessment of synchronic, heterochronic, and metastatic lesions in most patients was found, thereby improving staging accuracy. NGS targeting can identify genetic alterations of therapeutic significance. A comprehensive molecular evaluation allows the unambiguous delineation of clonal relationships among tumors [13]. Daryn's results suggest that gene sequencing technologies are potentially a more accurate diagnostic and

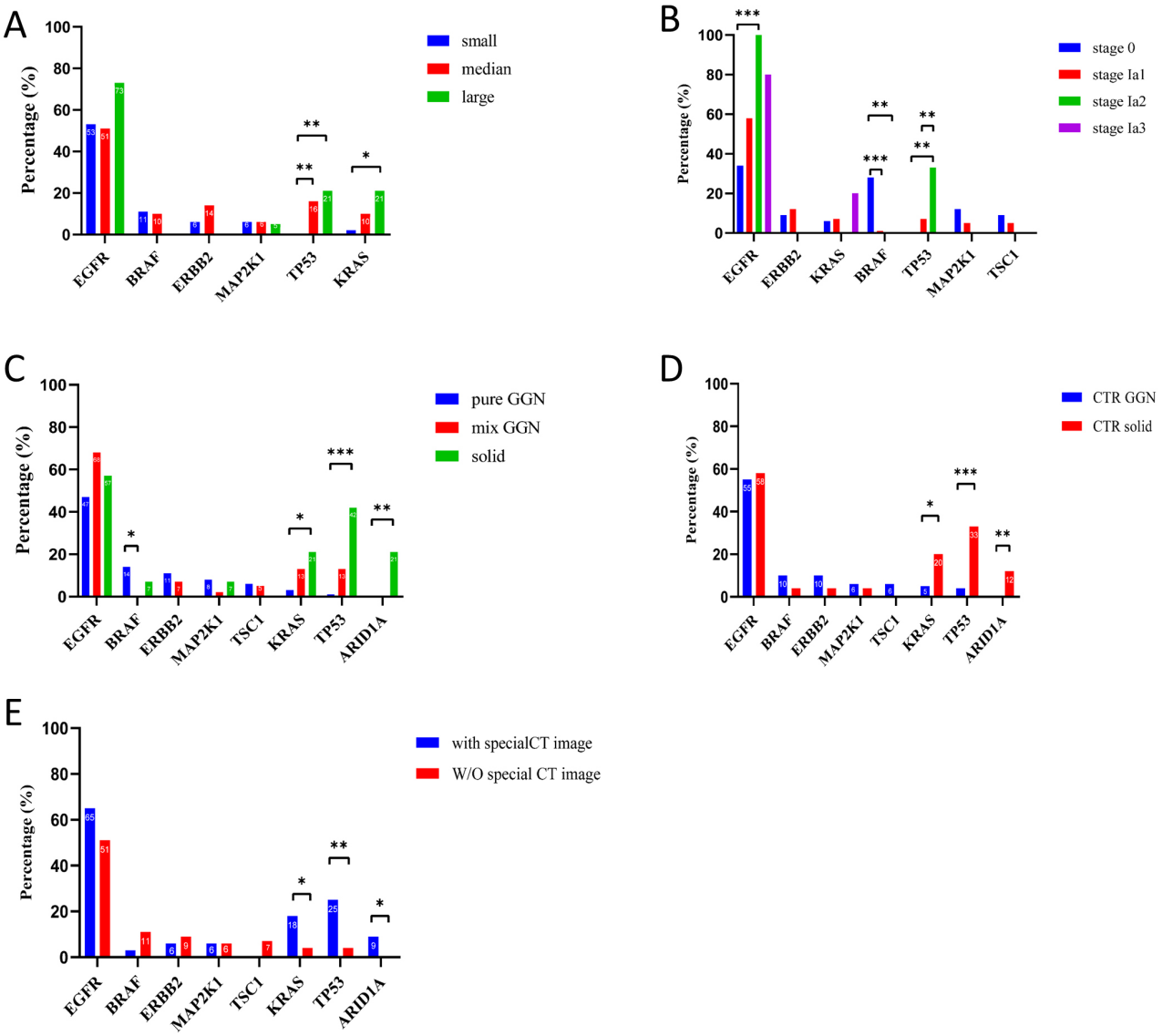

Fig. 4. Analysis between different clinical features and genetic mutations. (A) Nodules of different sizes main genetic analysis. Small, tumor size <5 mm; Median, tumor size 5–15 mm; Large, tumor size >15 mm. (B) Nodules in different stages primary genetic analysis. (C) Nodules of different CT components main genetic analysis. (D) Nodules of different CTR primary genetic analysis. (E) Nodules with or without special imaging manifestations primary genetic analysis. $^{*}p < 0.05$; $^{**}p < 0.01$; $^{***}p < 0.001$.

prognostic tool than traditional histopathologic evaluation in patients with suspected MPLCs, which could better guide treatment and outcomes prediction [14].

Chang *et al.* [15] compared the results of prospective histological predictions with subsequent NGS results, a comprehensive analysis of cancer target mutations (MSK-IMPACT) NGS. This study covered up to 468 cancer-associated genes, used to distinguish between IM and MPLC in clinical practice. Using the clonal relationship, they established by a large NGS panel, as the molecular gold standard, the accuracy and defects of MPLC. In addition, IM histological predictions were analyzed, and the clinicopathological and genomic features contributing to the clinical prediction of NSCLC clonality started being elucidated. In this study we performed NGS testing on 114 sample tissues, including 425 cancer-related genes, with *EGFR* gene as the highest rate of mutation of the among all samples. Followed by *TP53*, *ERBB2*, the median number of mutations was = 2 in patients with multiple nodules in the lungs, and the average number of mutations was = 2.79. Among them, *BRD4* co-occurred significantly with *LRP1B*/*DOT1L*, and *ARID1A* with *DOT1L*. Among the 11 drug target genes concerned in non-small cell lung cancer, the incidence of *EGFR* mutations accounted for 55.3% in 114 cases of multiple nodules, followed by *ERBB2*, *BRAF*, *KRAS*. Fusion mutations were rare. Similar to previous studies [13,16]. However, other studies found *KRAS* mutations to be the most common, followed by *TP53*, *EGFR*,

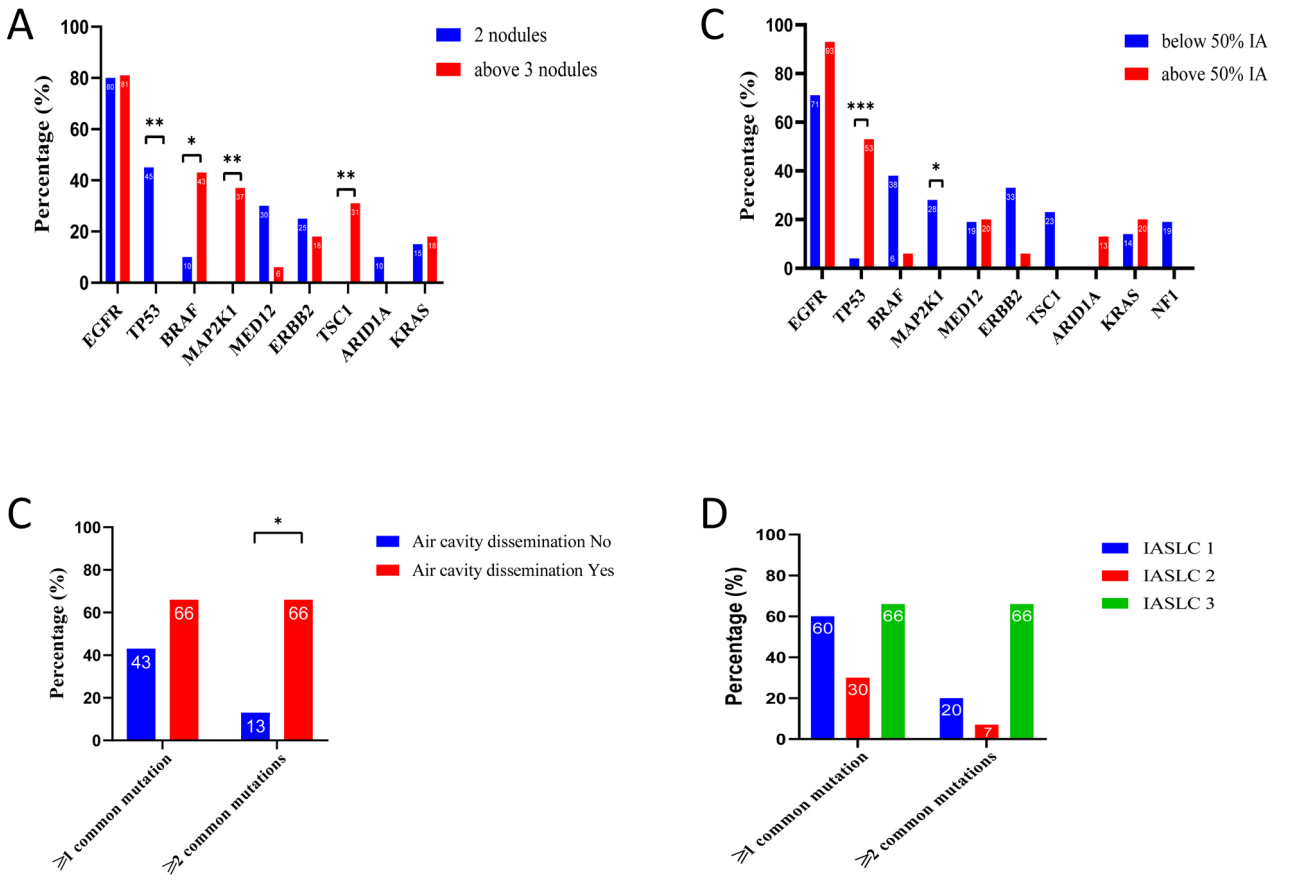

Fig. 5. Analysis of clinical features with genetic mutations in 36 patients. (A) Differences between the main genes grouped by the number of different nodules. (B) Differences between the main genes grouped by different IA proportions. (C) Differences in co-mutations with or without air cavity-disseminated nodules. (D) Differences in co-mutations of patients with different highest pathological grades. $^{*}p < 0.05$; $^{**}p < 0.01$; $^{***}p < 0.001$.

MET, and *PIK3CA*, which were very different from our results [14]. Hu *et al.* [16] showed that the *EGFR* mutation was mutually exclusive with *ERBB2*, *BRAF*, *KRAS*, and *MAP2K1* mutations while coexisting significantly with the *TP53* and *RBM10* mutations. In our study, *BRD4* co-occurred significantly with *LRP1B*/*DOT1L* and *ARID1A* with *DOT1L*.

EGFR mutations are more common in Asians. Exon 19 deletion is the most common [17], followed by L858R as a known hotspot mutation [18]. Li *et al.* [19] found a unique *EGFR* mutation signatures in a large cohort of MPLC probands. In our study, exon 21 mutation accounted for 58% of all *EGFR* mutations, of which the L858 locus accounted for 77%. Exon 19 mutations accounted for 12% of *EGFR* mutations (Fig. 2A). Mansuet's [20] study found significant differences between IM patients and MPLC patients in smoking history, the time interval between tumors, tumor location, lymph node involvement, and mutational status of *EGFR* and *KRAS*. The literature reports that in 65 cases of non-small cell lung cancer patients with *BRAF* mutations (*BRAF* V600E) accounted for the largest proportion of advanced NSCLC mutations (nearly 83%). *KRAS* G12C accounts for the largest proportion of late NSCLC *KRAS* mutations (close to 30%) [21,22]. In our study, V600E mutation accounted for only 10% of *BRAF* mutations, of which G12C accounted for about 18% of *KRAS* mutations (Fig. 2B,C). Hu *et al.* [16] indicated that *EGFR* p.L858R and exon 19del accounted for 38.46% and 21.89% of *EGFR* mutations, respectively; The most common mutant subtype of *ERBB2* is exon 20ins (21/31, 67.74%). V600E mutations account for 6.25% of *BRAF* mutations. Their result is close to our findings. Thus, it is noted that there are significant differences in the frequency of mutations in multiple lung cancer and advanced lung cancer. Pei *et al.* [13] found that the *EGFR*, *TP53*, *RBM10*, *ERBB2*, and *CDKN2A* mutations frequencies exhibited significant differences between early and advanced-stage NSCLCs. Their results support the adoption of a large panel to supplement histology to strongly discriminating NSCLC clonal relationships in clinical practice.

TMB is a predictive and prognostic biomarker for immune checkpoint inhibitors (ICIS) to treat multiple solid tu-

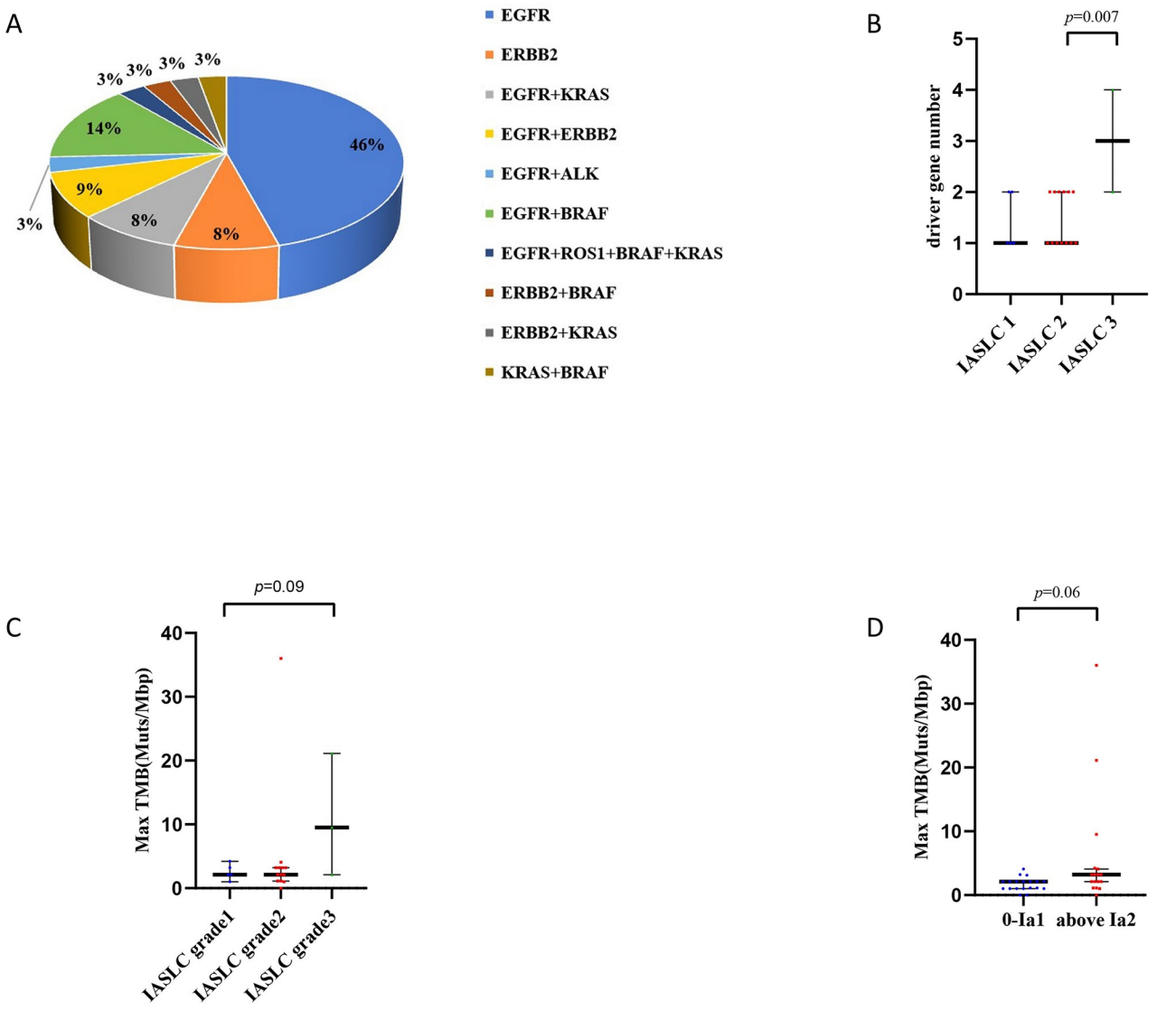

Fig. 6. Frequency of driver gene mutations and the highest TMB distribution in 36 patients. (A)Drive gene mutations in 36 patients' frequency. (B) Mutations in the driver gene in patients with different IASLC grades. (C) The highest TMB distribution of patients with different IASLC classifications. (D) The highest TMB distribution in patients with different stages.

mors [23], with an overall low TMB and a median TMB of 1.1 MUTS/Mb is present in patients with multiple nodules in the lungs (Fig. 2E). Chang *et al.* [15] recruited 37 patients with MPLC with an average TMB of 7.0 (0–41.2) MUTS/Mb, significantly higher than the TMB (1.1 MUTS/Mb) in our study. In Hu's [16] study, MPLC often showed low TMB (1.92), consistent with our results. In addition, we found that TMB was higher distributed in IA, >15 mm, CTR >0.5, and solid nodules. For early-stage lung cancer, tumors with *EGFR* mutations are more aggressive than wild-type *EGFR* tumors and they may be accompanied by more mutations. This may explain higher TMB levels in *EGFR*-mutated cancers [16]. In our study, the TMB of the *EGFR* gene mutation was higher but not statistically significant. Specific gene and concomitant mutations are closely related to TMB in MPLC, which may help identify patients benefiting from immunotherapy.

ARID1A is expressed in non-small cell lung cancer at rates of 1.2% to 7.5% [24–26], consistent with our research. Previous studies have found that abnormal *ARID1A* expression is associated with poor overall survival in patients with *ARID1A*-mutated non-small cell lung cancer [25–27]. Zhang *et al.* [28] found that silencing *ARID1A* by siRNA (small interfering RNA) promotes lung cancer cell proliferation and colony formation capacity, inhibits paclitaxel-induced apoptosis, reduces *ARID1A* expression in non-small cell lung cancer, and is significantly associated with lymph node metastasis and TNM staging. *ARID1A* mutations have been reported to be associated with poor prognosis in breast invasive micropapillary carcinoma and

micropapillary urothelial carcinoma [29,30]. We found that *ARID1A* mutations were significantly higher in IA containing solid/micro-papillary malignancy in multiple primary lung adenocarcinomas. This finding suggests that these patients with MPLC may have a poor prognosis. Members of the *ARID* family may serve as new biomarkers for immune checkpoint inhibitor treatment of malignant tumors. Cancer patients carrying mutations in *ARID1A* may benefit more from cancer immunotherapy.

When patients were studied as study individuals, the proportion of patients with *EGFR* mutations was higher (80.6%), followed by *BRAF* (25%), *TP53* (25%), and *ERBB2* (22.2%). Overall, 97.2% had driver gene mutations. The number of drive gene mutations ranged from 1 to 4. However, our study did not find a significant association between the distribution of the number of gene mutations in patients and the diameter, location, and stage. Among patients with multiple nodules, 47% had co-mutant genes, and 21% had more than two co-mutations. More than 2 co-mutant genes were significantly enriched in patients with air cavity dissemination, suggesting that co-mutant genes may be more likely to occur in patients with air cavity dissemination.

Patients who share a driver gene may develop more aggressive cancers. MPLCs are more common in non-smoking women under 60, manifesting primarily as ground glass shadows, adenocarcinoma, and stage I lung lesions [16]. In our study, the first 4 co-mutation sites in co-mutant genes were functional mutations, except for *EGFR* M1007T. There were 9 patients with *EGFR* co-mutation with 11 co-mutation sites, of which L858R accounted for the largest proportion, considering the high incidence of L858R in the population, the high incidence of multiple nodules L858R here may be a probability event (**Supplementary Fig. 2B**). In addition, it was found a higher trend in the number of gene mutations, TMB, and co-mutation in patients with IASLC level 3. This suggests that patients with IASLC grade 3 multiple lung adenocarcinomas may have poorer prognosis.

It is essential to distinguish MPLC and IM at molecular level. Takahashi *et al.* [31] used NGS to target and sequence 20 lung cancer-associated oncogenes on 82 tumors of 37 surgically removed MPLC patients. In their study, in histopathology for MPLC cases (n = 17), mutation evaluation yielded an inconsistent diagnosis in 47% of the cases. Chang *et al.* [15] applied 341–468 gene MSK-Impact NGS analysis method to assess 4119 NSCLCs. Forward-looking histological predictions were inconsistent with NGS by 22%. The prediction inconsistencies with IM were 44%, which was significantly higher than that of MPLC (12%). These results suggest that, in addition to histopathological evaluation, multiple mutation analysis may be a use as a complementary tool to distinguishing between MPLC and IM [31].

Patel *et al.* [32] assessed whether the use of 50 genes NGS could be used to facilitate the discrimination between IM and MPLC. This was the first study to correlate molecular predictions of NGS lineage allocation with clinical outcomes in patients with multifocal lung cancer. The results were consistent with previous findings, and these individuals were examined for consistency in the mutant states of *KRAS*, *EGFR*, *BRAF*, and *TP53* between primary and metastatic lung cancers [33]. Our results showed a total of 17 patients with co-mutations, of which the top 5 genes accounted for *EGFR*, *KRAS*, *ERBB2*, *TP53*, *DOT1L* (**Supplementary Fig. 2A**). In addition, according to the TCGA (The Cancer Genome Atlas) database, some rare gene mutations co-mutate, such as *STK11* (F354L), *MET* T1010I, *KRAS* G12S and *PIK3CA* H1047R. This suggests the possibility of intrapulmonary metastases [14]. Some studies have also shown that mutation profiles quality assessment in pairs of primary and metastatic lung cancer specimens and multiple metastatic lung cancer specimens by NGS has resulted in a high degree of consistency within backbone driver mutations. The backbone driver mutations in the *EGFR*, *KRAS*, or *BRAF* genes were consistent in 15 patients with multiple metastasis. However, they were inconsistent in 32 pairs of primary and three pairs of metastatic samples [34]. In MPLC, the driver mutation profile is mutually exclusive among individual tumors, while it is consistent between metastasized tumors and primary lesions [35].

It was found that most MPLC patients (35/36, 97.2%) have at least one nodule with a driver gene mutation, indicating that the driver gene mutation is prevalent in MPLC patients. WJOG13019L is the first large-scale, real-world study to implement NGS as a companion diagnostic system in clinical practice. It revealed NSCLC genetic mutation profile using the Oncomine Dx Target Test Multi-CDx System. The success rate of genetic alteration testing of the four driver genes *EGFR*, *ALK*, *ROS1*, and *BRAF* was 80.1% [36]. These results show that optimizing sample size and quality may improve the clinical application of drive gene testing [36].

Multiple lung adenocarcinoma gene mutations frequency is generally low, and large panel NGS can determine more, broader, and more complete gene loci at once, which further help understanding multiple lung adenocarcinomas gene mutations. The main limitations of the large panel NGS platform include availability, cost, and turnaround time. Due to the cost of implementation and the considerable demand for bioinformatics, computing resources, and personnel to analyze and interpret data, not all institutions currently offer NGS testing.

The vast majority of MPLC patients included in this study were in the early stage of the disease. It is difficult to obtain the sample tissue of patients with advanced MPLC, so the gene map of MPLC in the middle and advanced stages still needs to be improved. In addition, the

number of MPLC with micropapillary/solid components is small, and the prognosis and follow-up of *ARID1A*-mutated MPLC with micropapillary/solid components require studies with larger sample size.

Conclusions

MPLC has a unique genetic mutation characteristic that differs from advanced patients and usually presents low TMB. Comprehensive NGS helps diagnosing of MPLC and guides MPLC clinical treatment. *ARID1A* is significantly enriched in IA nodules containing micro-papillary/solid components in MPLC patients, which may serve to detect MPLC patients with high risk of poor prognosis.

Abbreviations

MPLC, multiple primary lung cancer; NGS, next-generation sequencing; CT, computed tomography; *EGFR*, epidermal growth factor receptor; IM, intrapulmonary metastases; TMB, tumor mutation burden; AIS, adenocarcinoma in situ; MIA, minimally invasive adenocarcinoma; IA, invasive adenocarcinoma; IASLC, International Association for the Study of Lung Cancer; *KRAS*, Kirsten rat sarcoma viral oncogene; NSCLC, non-small cell lung cancer; CTR, consolidation tumor ratio; SNV, single nucleotide variant; CNV, copy number variation; GGN, ground glass nodule; *TP53*, tumor protein 53; *ERBB2*, Erb-B2 Receptor Tyrosine Kinase 2; *BRD4*, Bromodomain-Containing Protein 4; *LRP1B*, low density lipoprotein-related protein 1B; *ARID1A*, AT-rich interaction domain 1A; *BRAF*, v-Raf murine sarcoma viral oncogene homolog B1; *ROS1*, c-ros oncogene 1; *ALK*, anaplastic lymphoma kinase; *MET*, mesenchymal-epithelial transition factor; *RET*, rearranged during transfection; *NTRK*, neurotrophic tyrosine receptor kinase; *NF1*, Neurofibromin 1; *MAP2K1*, mitogen-activated protein kinase kinase 1; ICIS, immune checkpoint inhibitors; UICC, International Union Against Cancer; TNM, Tumor Node Metastasis; IDT, Integrated DNA Technologies; COSMIC, Catalogue of Somatic Mutations in Cancer; MUTS/Mb, Mutations per Megabase; TERT, telomerase reverse transcriptase; *TSC1*, Tuberous Sclerosis Complex 1.

Availability of Data and Materials

The datasets presented in this study can be found in Genome Sequence Archive (GSA) database with the accession numbers of HRA003776, further inquiries can be directed to the corresponding author.

Author Contributions

ZL and GZ—contributed to acquisition of data, data analysis, and article writing; WW and BD—contributed to acquisition of data, data analysis, and article editing; CC and FL—contributed to acquisition of data and data analysis; GL and YL—contributed to data analysis and article editing; ZL and HL—contributed to data analysis and article editing; GM—contributed to data analysis and article editing; HM—contributed to study conception and coordination and article editing. All authors contributed to editorial changes in the manuscript. All authors read and approved the final manuscript. All authors have participated sufficiently in the work and agreed to be accountable for all aspects of the work.

Ethics Approval and Consent to Participate

This study was reviewed and approved by the Clinical Trial Ethics Committee of the Affiliated Hospital of Guangdong Medical University, Zhanjiang, China (approval number: PJKT2023026) and written informed consent was given by the patient. This report was prepared in accordance with the Helsinki Declaration.

Acknowledgment

The authors wish to acknowledge Dr. Yang, Dr. Zhu and Dr. Hong, professor of Nanjing Geneseeq Technology Inc., for their help in taking pathological samples for genetic testing.

Funding

This work was supported by grants from the Key Clinical Research Projects of the Affiliated Hospital of Guangdong Medical University (No. LCYJ2018B001).

Conflict of Interest

The authors declare no conflict of interest.

Supplementary Material

Supplementary material associated with this article can be found, in the online version, at https://doi.org/10.24976/Discov.Med.202335175.14.

References

[1] Sung H, Ferlay J, Siegel RL, *et al*. Global Cancer Statistics 2020: GLOBOCAN Estimates of Incidence and Mortality Worldwide for 36 Cancers in 185 Countries. *CA Cancer J Clin*. 2021;71(3):209–249. doi: 10.3322/caac.21660

[2] Xia C, Dong X, Li H, *et al*. Cancer statistics in China and United States, 2022: profiles, trends, and determinants. *Chin Med J (Engl)*. 2022;135(5):584–590. doi: 10.1097/CM9.0000000000002108

[3] Chen W, Zheng R, Baade PD, *et al*. Cancer statistics in China, 2015. *CA Cancer J Clin*. 2016;66(2):115–132. doi: 10.3322/caac.21338

[4] Gazdar AF, Minna JD. Multifocal lung cancers—clonality vs field cancerization and does it matter? *J Natl Cancer Inst*. 2009;101(8):541–543. doi: 10.1093/jnci/djp059

[5] Chen C, Huang X, Peng M, Liu W, Yu F, Wang X. Multiple primary lung cancer: a rising challenge. *J Thorac Dis*. 2019;11(Suppl 4):S523–S536. doi: 10.21037/jtd.2019.01.56

[6] Smith-Bindman R, Miglioretti DL, Johnson E, *et al*. Use of diagnostic imaging studies and associated radiation exposure for patients enrolled in large integrated health care systems, 1996–2010. *JAMA*. 2012;307(22):2400–2409. doi: 10.1001/jama.2012.5960

[7] Trousse D, Barlesi F, Loundou A, *et al*. Synchronous multiple primary lung cancer: an increasing clinical occurrence requiring multidisciplinary management. *J Thorac Cardiovasc Surg*. 2007;133(5):1193–1200. doi: 10.1016/j.jtcvs.2007.01.012

[8] Jiang L, He J, Shi X, *et al*. Prognosis of synchronous and metachronous multiple primary lung cancers: systematic review and meta-analysis. *Lung Cancer*. 2015;87(3):303–310. doi: 10.1016/j.lungcan.2014.12.013

[9] Arai J, Tsuchiya T, Oikawa M, *et al*. Clinical and molecular analysis of synchronous double lung cancers. *Lung Cancer*. 2012;77(2):281–287. doi: 10.1016/j.lungcan.2012.04.003

[10] Schneider F, Derrick V, Davison JM, Strollo D, Incharoen P, Dacic S. Morphological and molecular approach to synchronous non-small cell lung carcinomas: impact on staging. *Mod Pathol*. 2016;29(7):735–742. doi: 10.1038/modpathol.2016.66

[11] Wang S, Wang Z. Meta-analysis of epidermal growth factor receptor and KRAS gene status between primary and corresponding metastatic tumours of non-small cell lung cancer. *Clin Oncol (R Coll Radiol)*. 2015;27(1):30–39. doi: 10.1016/j.clon.2014.09.014

[12] Frampton GM, Fichtenholtz A, Otto GA, *et al*. Development and validation of a clinical cancer genomic profiling test based on massively parallel DNA sequencing. *Nat Biotechnol*. 2013;31(11):1023–1031. doi: 10.1038/nbt.2696

[13] Pei G, Li M, Min X, *et al*. Molecular Identification and Genetic Characterization of Early-Stage Multiple Primary Lung Cancer by Large-Panel Next-Generation Sequencing Analysis. *Front Oncol*. 2021;11:653988. doi: 10.3389/fonc.2021.653988

[14] Goodwin D, Rathi V, Conron M, Wright GM. Genomic and Clinical Significance of Multiple Primary Lung Cancers as Determined by Next-Generation Sequencing. *J Thorac Oncol*. 2021;16(7):1166–1175. doi: 10.1016/j.jtho.2021.03.018

[15] Chang JC, Alex D, Bott M, *et al*. Comprehensive Next-Generation Sequencing Unambiguously Distinguishes Separate Primary Lung Carcinomas from Intrapulmonary Metastases: Comparison with Standard Histopathologic Approach. *Clin Cancer Res*. 2019;25(23):7113–7125. doi: 10.1158/1078-0432.CCR-19-1700

[16] Hu C, Zhao L, Liu W, *et al*. Genomic profiles and their associations with TMB, PD-L1 expression, and immune cell infiltration landscapes in synchronous multiple primary lung cancers. *J Immunother Cancer*. 2021;9(12):e003773. doi: 10.1136/jitc-2021-003773

[17] Mitsudomi T, Kosaka T, Yatabe Y. Biological and clinical implications of EGFR mutations in lung cancer. *Int J Clin Oncol*. 2006;11(3):190–198. doi: 10.1007/s10147-006-0583-4

[18] Mok TS, Wu YL, Thongprasert S, *et al*. Gefitinib or carboplatin-paclitaxel in pulmonary adenocarcinoma. *N Engl J Med*. 2009;361(10):947–957. doi: 10.1056/NEJMoa0810699

[19] Li C, Wang Y, Su K, *et al*. Presentation of *EGFR* mutations in 162 family probands with multiple primary lung cancer. *Transl Lung Cancer Res*. 2021;10(4):1734–1746. doi: 10.21037/tlcr-20-1001

[20] Mansuet-Lupo A, Barritault M, Alifano M, *et al*. Proposal for a Combined Histomolecular Algorithm to Distinguish Multiple Primary Adenocarcinomas from Intrapulmonary Metastasis in Patients with Multiple Lung Tumors. *J Thorac Oncol*. 2019;14(5):844–856. doi: 10.1016/j.jtho.2019.01.017

[21] Liu SY, Sun H, Zhou JY, *et al*. Clinical characteristics and prognostic value of the *KRAS G12C* mutation in Chinese non-small cell lung cancer patients. *Biomark Res*. 2020;8:22. doi: 10.1186/s40364-020-00199-z

[22] Tian P, Zeng H, Ji L, *et al*. Lung adenocarcinoma with ERBB2 exon 20 insertions: Comutations and immunogenomic features related to chemoimmunotherapy. *Lung Cancer*. 2021;160:50–58. doi: 10.1016/j.lungcan.2021.07.014

[23] Sha D, Jin Z, Budczies J, Kluck K, Stenzinger A, Sinicrope FA. Tumor Mutational Burden as a Predictive Biomarker in Solid Tumors. *Cancer Discov*. 2020;10(12):1808–1825. doi: 10.1158/2159-8290.CD-20-0522

[24] Sun S, Li Q, Zhang Z, *et al*. SMARCA2 deficiency in NSCLC: a clinicopathologic and immunohistochemical analysis of a large series from a single institution. *Environ Health Prev Med*. 2022;27(0):3.

[25] Hung YP, Redig A, Hornick JL, Sholl LM. ARID1A mutations and expression loss in non-small cell lung carcinomas: clinicopathologic and molecular analysis. *Mod Pathol*. 2020;33(11):2256–2268. doi: 10.1038/s41379-020-0592-2

[26] Sun D, Tian L, Zhu Y, *et al*. Subunits of ARID1 serve as novel biomarkers for the sensitivity to immune checkpoint inhibitors and prognosis of advanced non-small cell lung cancer. *Mol Med*. 2020;26(1):78. doi: 10.1186/s10020-020-00208-9

[27] Sun D, Zhu Y, Zhao H, *et al*. Loss of ARID1A expression promotes lung adenocarcinoma metastasis and predicts a poor prognosis. *Cell Oncol (Dordr)*. 2021;44(5):1019–1034. doi: 10.1007/s13402-021-00616-x

[28] Zhang Y, Xu X, Zhang M, *et al*. ARID1A is downregulated in non-small cell lung cancer and regulates cell proliferation and apoptosis. *Tumour Biol*. 2014;35(6):5701–5707. doi: 10.1007/s13277-014-1755-x

[29] Onder S, Fayda M, Karanlık H, *et al*. Loss of ARID1A expression is associated with poor prognosis in invasive micropapillary carcinomas of the breast: A clinicopathologic and immunohistochemical study with long-term survival analysis. *Breast J*. 2017;23(6):638–646. doi: 10.1111/tbj.12823

[30] Li J, Lu S, Lombardo K, Monahan R, Amin A. ARID1A alteration in aggressive urothelial carcinoma and variants of urothelial carcinoma. *Hum Pathol*. 2016;55:17–23. doi: 10.1016/j.humpath.2016.04.006

[31] Takahashi Y, Shien K, Tomida S, *et al*. Comparative mutational evaluation of multiple lung cancers by multiplex oncogene mutation analysis. *Cancer Sci*. 2018;109(11):3634–3642. doi: 10.1111/cas.13797

[32] Patel SB, Kadi W, Walts AE, *et al*. Next-Generation Sequencing: A Novel Approach to Distinguish Multifocal Primary Lung Adenocarcinomas from Intrapulmonary Metastases. *J Mol Diagn*. 2017;19(6):870–880. doi: 10.1016/j.jmoldx.2017.07.006

[33] Sherwood J, Dearden S, Ratcliffe M, Walker J. Mutation status concordance between primary lesions and metastatic sites of advanced non-small-cell lung cancer and the impact of mutation testing methodologies: a literature review. *J Exp Clin Cancer Res*. 2015;34(1):92. doi: 10.1186/s13046-015-0207-9

[34] Murphy SJ, Harris FR, Kosari F, *et al*. Using Genomics to Differentiate Multiple Primaries from Metastatic Lung Cancer. *J Thorac Oncol*. 2019;14(9):1567–1582. doi: 10.1016/j.jtho.2019.05.008

[35] Higuchi R, Nakagomi T, Goto T, *et al*. Identification of Clonality through Genomic Profile Analysis in Multiple Lung Cancers. *J Clin Med*. 2020;9(2):573. doi: 10.3390/jcm9020573

[36] Sakata S, Otsubo K, Yoshida H, *et al*. Real-world data on NGS using the Oncomine DxTT for detecting genetic alterations in non-small-cell lung cancer: WJOG13019L. *Cancer Sci*. 2022;113(1):221–228. doi: 10.1111/cas.15176